Master's thesis
Your Field

Formation of cores by merging supermassive black holes

Joonas Suortti

July 12, 2019

Tutor: prof. Smith

Censors: prof. Smith
doc. Smythe

UNIVERSITY OF HELSINKI
Department of Something

PL 42 (Kuvitteellinen katu 1)
00014 Helsingin yliopisto

“Bachelor’s degrees make pretty good placemats if you get them laminated.”

—Jeph Jacques

HELSINGIN YLIOPISTO — HELSINGFORS UNIVERSITET — UNIVERSITY OF HELSINKI

Tiedekunta — Fakultet — Faculty	Laitos — Institution — Department
Faculty of Whatever	Department of Something

Tekijä — Författare — Author

Joonas Suortti

Työn nimi — Arbetets titel — Title

Formation of cores by merging supermassive black holes

Oppiaine — Läroämne — Subject

Your Field

Työn laji — Arbetets art — Level	Aika — Datum — Month and year	Sivumäärä — Sidoantal — Number of pages
Master's thesis	July 12, 2019	0 pages

Tiivistelmä — Referat — Abstract

Abstract goes here.

Avainsanat — Nyckelord — Keywords

Your keywords here

Säilytyspaikka — Förvaringsställe — Where deposited

Muita tietoja — övriga uppgifter — Additional information

Contents

1. Introduction

2. Theory

3. KETJU

4. Merger Simulations Using KETJU

We analyse the results of two simulation sets of galaxy mergers with central supermassive black holes, both done using the KETJU code by Mannerkoski et al. (2019) and Rantala et al. (2018). This is done in order to determine if merging SMBHs are able to cause the formation of cored galaxies, how the black hole masses affect the size of the core, and if the KETJU-code produces merger remnants comparable to observations.

4.1 Simulation Details

All of the different simulation runs analysed, use merger progenitor galaxies from the same progenitor pool. There are seven different progenitors in total. Six of them (BH-1 - BH-6) contain central supermassive black holes, with the BH masses varying from $8.5 \times 10^8 M_\odot$ to $8.5 \times 10^9 M_\odot$. The seventh progenitor (BH-0) doesn't have an SMBH in its centre, and is included for the sake of comparison. The detailed masses of the progenitors' central SMBHs are listed in table 4.1. Apart from the SMBH masses however, all of the progenitor galaxies have identical physical properties. These properties are described in table 4.2, while the reasoning behind them is explained in Rantala et al. (2018) (do I have to go into same amount of detail as in the paper?).

Progenitor	$M_\bullet$ $[\times 10^9 M_\odot]$
BH-0	-
BH-1	0.85
BH-2	1.7
BH-3	3.4
BH-4	5.1
BH-5	6.8
BH-6	8.5

Table 4.1: Central SMBH masses of the progenitors used in the analysed simulations.

Alongside the physical properties, the distributions of the different particles that make up the progenitor galaxies are also identical. Not counting the central point mass SMBH, all of the particles are distributed according to a Dehnen density-potential model (Dehnen, 1993):

$$\rho(r) = \frac{(3-\gamma)M}{4\pi} \frac{a}{r^\gamma (r+a)^{4-\gamma}}, \tag{4.1}$$

$$\phi(r) = \frac{GM}{a} \times \begin{cases} -\frac{1}{2-\gamma}\left[1 - \left(\frac{r}{r+a}\right)^{2-\gamma}\right] & \gamma \neq 2 \\ \ln \frac{r}{r+a} & \gamma = 2 \end{cases}, \tag{4.2}$$

where M is the total mass, a is a scaling radius, and γ is the central slope of the profile. The fundamental difference between the models describing the distribution of the rest of the particles, i.e. stellar and dark matter particles, is that for stellar particles the value used for γ is 3/2, while for the dark matter particles $\gamma = 1$.

While the merger progenitor galaxies are the same, the initial conditions of the simulations are quite different. The Mannerkoski et al. (2019) simulations comprise of four subsequent runs, where, initially the progenitor galaxy BH-6 (table 4.1), and later the remnant of the previous merger, is merged with the progenitor BH-2. On

$M_\star$ $[\times 10^{11} M_\odot]$	R_e [kpc]	$M_{\rm DM}$ $[\times 10^{13} M_\odot]$	$f_{\rm DM}(r_{1/2})$	$N_\star$	$N_{\rm DM}$
4.15	7	7.5	0.25	4.15×10^6	1.0×10^7

Table 4.2: The physical properties, constant throughout the different progenitor galaxies:
$M_\star$: Stellar mass
R_e: Effective radius
$M_{\rm DM}$: Mass of the dark matter halo
$f_{\rm DM}(r_{1/2})$: Fraction of dark matter mass compared to stellar mass inside the effective radius
$N_\star$: Number of stellar particles
$N_{\rm DM}$: Number of dark matter particles

the other hand, the simulations done by Rantala et al. (2018) contain simply seven different mergers between two of the same progenitor galaxies.

The results gathered from the two sets of simulations also differ from each other. From the simulations done by Mannerkoski et al. (2019); the locations, velocities and masses of the central SMBHs are saved. The data comes from time steps starting from when the semi-major-axis of the merging SMBH binary is $a \lesssim 5000 R_s$ (R_s is the Schwarzschild radius) up until the end of the simulation. The simulation results of Rantala et al. (2018), however, consists of not only the properties of the black holes, but also the stellar particles and dark matter particles, in the form of a single snapshot at the simulation time $t = 2$Gyr. Due to the distinct difference between the type of results gained from the two different simulation sets (and for simplicity's sake), we will from now on be calling the simulations from Mannerkoski et al. (2019) "Runs", and the ones from Rantala et al. (2018) "Snapshots" (table 4.3).

Mannerkoski et al. (2019)			Rantala et al. (2018)		
Run	$M_{\bullet,1}[10^9 M_\odot]$	$M_{\bullet,2}[10^9 M_\odot]$	Snapshot	$M_{\bullet,1}[10^9 M_\odot]$	$M_{\bullet,2}[10^9 M_\odot]$
1	8.5	1.7	0	-	-
2	10.2	1.7	1	0.85	0.85
3	11.9	1.7	2	1.7	1.7
4	13.6	1.7	3	3.4	3.4
			4	5.1	5.1
			5	6.8	6.8
			6	8.5	8.5

Table 4.3: Central SMBH masses of the progenitors used in the different simulation runs.

4.2 Black Hole Trajectories

4.3 Core Size Measurements

In order to check if a merger remnant is cored or not, we first have to calculate their surface brightness profiles. As the "Runs" don't contain stellar data, we use the "Snapshots" for the core analysis.

We calculate the surface brightness profiles from the snapshots by: changing the coordinate system to centre-of-mass coordinates, projecting the stellar particles onto a plane, and calculating masses inside logarithmically space radial bins to get a radial mass surface density profile. We then do the aforementioned calculations 100 times from random viewing angles and calculate the azimuthal average of the profiles. This allows us to form a smooth mass surface density profile, which we then turn into a surface brightness profile by assuming a mass-to-light ratio of $M/L = 4$ (Rantala et al., 2018). In figure 4.3, one can see example surface brightness profiles for all of the snapshots. Looking at the different curves, it seems like the presence

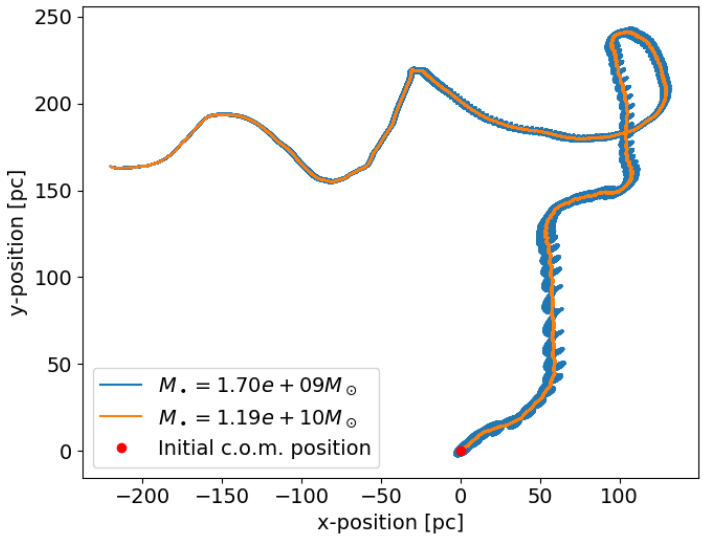

Figure 4.1: The trajectories of the black holes during "run 3" of the simulation. The coordinates are centred on the initial location of the centre-of-mass of the black hole system. The orange and blue lines show the paths taken by the smaller and larger black holes respectively during the simulation. Both paths show clear spiral patterns which become smaller and smaller as the simulation proceeds. The paths end at the location where the black holes merge, i.e. where the distance between them is below the specific threshold.

of central SMBHs in the progenitor galaxies does cause some kind of brightness deficiency near the galactic centre of the remnant's surface brightness profile. Not only that, the higher the mass of the central black holes in the progenitor galaxies, the larger the surface brightness deficiency seems to be.

The surface brightness profiles mentioned above do seem to indicate the presence of cores in the merger remnants with merging SMBH binaries. Determining the precise size of the core requires us to find the exact location where the deviations from the expected power-law profile start. This can be done by fitting the calculated profile with a model that is a combination of two power laws, a shallow inner power-law and steeper outer power-law. The location where the power laws change, i.e. the break radius r_b is equivalent to the radius of the core.

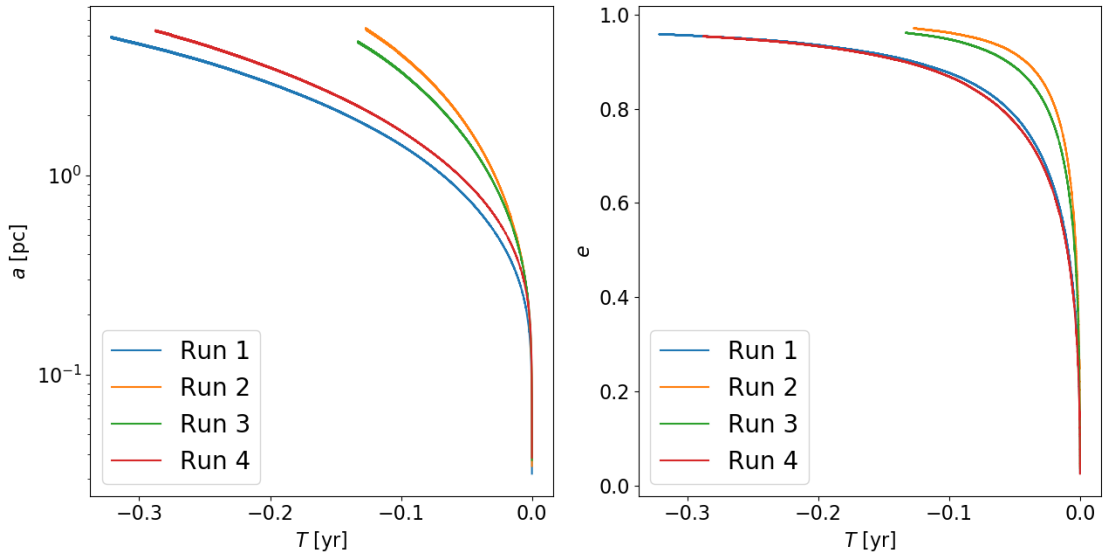

Figure 4.2: The semi-major axes (left) and eccentricities (right) of the black hole systems in simulation runs 1-4 as a function of time. The zero position on the x-axis corresponds to the point of time in the simulation, where the black hole merging event happens.

There are two commonly used options for modelling the surface brightnes profiles. The first one is the core-Sérsic profile (Graham et al., 2003a), which can be expressed using the following equation:

$$\mu(r) = \mu' \left[1 + \left(\frac{r_b}{r}\right)^{\alpha}\right]^{\gamma/\alpha} \exp\left\{-b_n \left[\left(r^{\alpha} + r_b^{\alpha}\right)/r_e^{\alpha}\right]^{1/(\alpha n)}\right\}, \tag{4.3}$$

where r_b is the break radius (i.e. the core radius), γ is the logarithmic slope of the inner power-law, α controls the sharpness of the transition between the two power-laws, r_e and n are the effective half-mass radius and the Sérsic index of the outer power-law, and the normalization factor μ' is defined by:

$$\mu' = \mu_b 2^{-\gamma/\alpha} \exp\left[b_n \left(2^(1/\alpha) r_b/r_e\right)^{1/n}\right], \tag{4.4}$$

where μ_b is the surface brightness at the break radius.

The second option for determining the core radius through profile fitting, is using the so called Nuker profile (Lauer et al., 1995):

$$\mu(r) = 2^{(\beta-\gamma)/\alpha} \mu_b \left(\frac{r_b}{r}\right)^{\gamma} \left[1 + \left(\frac{r}{r_b}\right)^{\alpha}\right]^{(\gamma-\beta)/\alpha}, \tag{4.5}$$

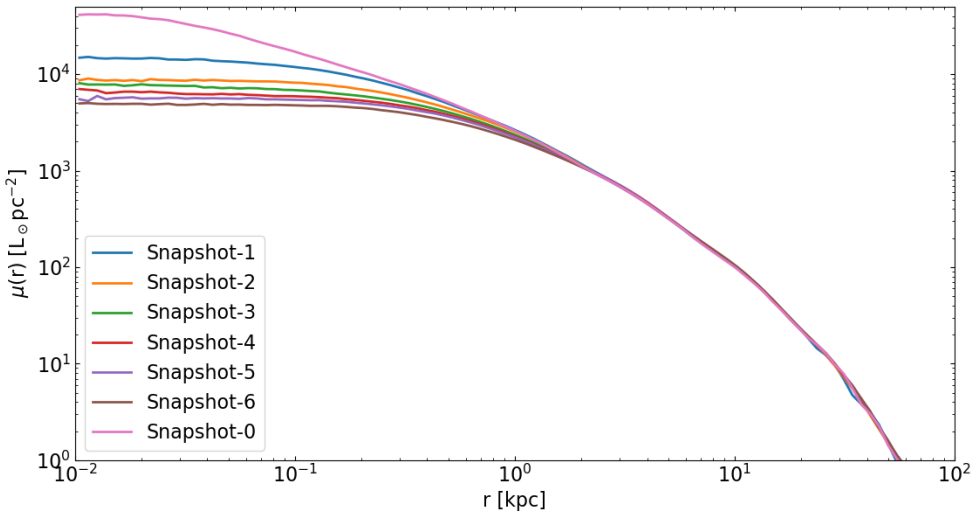

Figure 4.3: Surface brightness profiles of all of the simulated merger remnants. The profiles were calculated by dividing the remnants into 100 radial bins, and averaging the surface brightness inside the bins through 100 random viewing angles. The luminosity of the particles was estimated by assuming a mass-to-light ratio of $M/L = 4$.

where r_b is once again the break radius (core radius), μ_b is the surface brightness at the core radius, β and γ are the logarithmic slopes of the power-laws inside and outside of the break radius respectively, and α is the sharpness of the transition between the two slopes.

We use the "Levenberg-Marquardt" algorithm to fit core-Sérsic and Nuker models to surface brightness profiles that we have calculated. Figure 4.4 shows a comparison of the resulting fits for snapshot 3 (refer to table 4.3), while figures A.2 and A.3, located in the appendix, show the fits for every snapshot containing SMBH binaries. The values of the best-fit parameters are written on the figures, and looking at them, it is clear that the exact value of the best-fit break radius, i.e. the core radius estimate, depends quite heavily on the model used.

Which model is better for estimating the size of the core is up for debate Lauer et al. (2007b); Dullo and Graham (2012). While the rms of the relative residuals

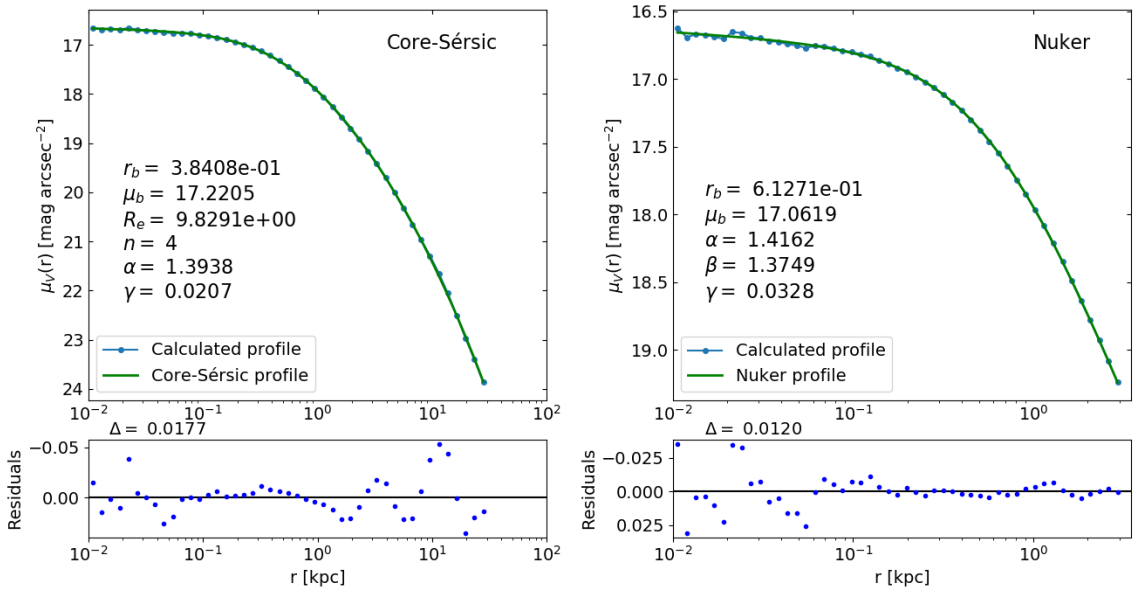

Figure 4.4: Core-Sérsic and Nuker profile fits of surface brightness profiles calculated from Snapshot 3 (top-left and top-right figures). The best fit parameters are written on the figures, and are in the same units as the axes (i.e. r_b and R_e in kilo-parsecs, and μ_b in V-band magnitudes per arc-second squared). The relative residuals of the fits are plotted under their respective figures. The delta describes the root-mean-square of the residuals.

seems to be consistently marginally smaller for the Nuker model when compared to the rms for the core-Sérsic model (compare figures A.2 and A.3), one also has to take into account that in the Nuker model the best-fit value for r_b is highly dependent on the fitting range (Graham et al., 2003b). Furthermore, as stated by Rantala et al. (2018), the fitting range of the Nuker model has to be narrowed down closer to the galactic core, in order to get sensible values for all of the model parameters ($\alpha \lesssim 1$ might prevent the model from describing the profile as a combination of two power-laws).

It is also possible to estimate the size of the core without model fitting by using the so-called "cusp radius" r_γ, which is the radius at which the negative logarithmic slope of the surface brightness density γ' equals 1/2 (Carollo et al., 1997; Lauer et al., 2007a). The cusp radius r_γ is also an estimation for the location where the inner power-law of the profile changes into the outer power-law, and thus equates

to the core radius.

We calculate r_γ for all of the snapshots with SMBH binaries by calculating the first derivative (i.e. gradient) of the surface brightness profiles, and then using a "Nelder-Mead" minimization algorithm to find the radius, at which the gradient gets the value $-1/2$.

Figure 4.5 compares the core radius estimates from each of the three methods for every merger remnant from the snapshots. The break radii from the Nuker fits are consistently larger than the other core radius estimates, while also being the ones that, in general, agree least with the other values. However, a clear trend of, the size of the core growing with the masses of the central SMBHs of the merger progenitors, can be seen.

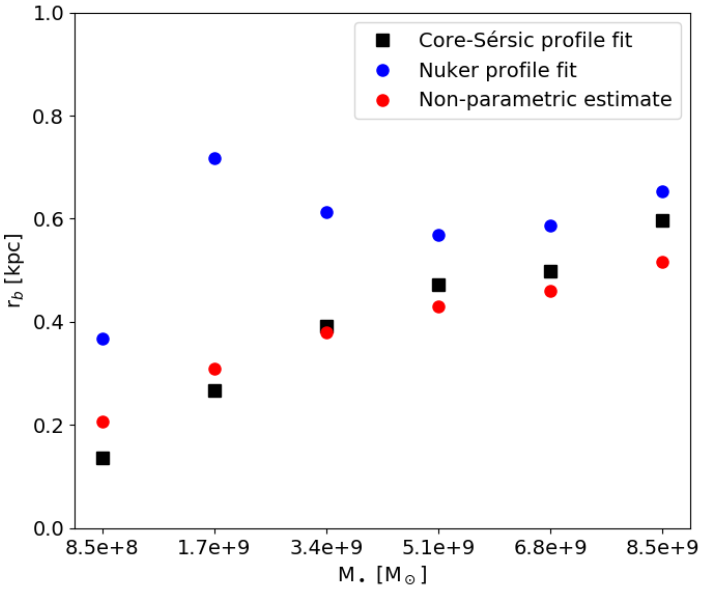

Figure 4.5: Comparison of core radii of the merger remnants, gained through three different methods: Core-Sérsic profile fitting (black squares), Nuker profile fitting (blue circles) and finding the "cusp radius" (red circles). The x-axis shows the masses of the central SMBHs of the merger progenitors.

4.4 Velocity Anisotropy

One way of adding to the evidence that a galaxy has experienced core scouring by binary black holes, is to study its velocity anisotropy profile defined in Binney and Tremaine (2008):

$$\beta(r) = 1 - \frac{\sigma_\theta^2 - \sigma_\phi^2}{2\sigma_r^2} = 1 - \frac{\sigma_t^2}{\sigma_r^2}, \tag{4.6}$$

where σ_θ, σ_ϕ and σ_r are velocity dispersions in the spherical coordinates, and $\sigma_t = \sqrt{(\sigma_\theta^2 + \sigma_\phi^2)/2}$ is the tangential velocity dispersion. The β parameter describes the relation between objects in radial and tangential orbits around the black hole binary, where a negative β shows an abundance of tangential orbits, and positive an abundance of radial orbits.

As the merging of two galaxies would cause a randomization of the stellar orbits, an area with negative β (largely tangential stellar orbits) in the merger remnant, would imply that the stars on radial orbits have been ejected from the system. It has been shown that hardening black hole binaries can eject stars on highly radial orbits from the galactic core, which then causes the outer orbits to become more radial (Quinlan and Hernquist, 1997; Milosavljević and Merritt, 2001; Thomas et al., 2014), and looking at figure 4.6, it seems like the same has happened in the simulations.

Figure 4.6 shows β-profiles calculated from the merger remnant simulation snapshots using equation 4.6. According to the profiles, the outer areas of the remnants are dominated by radial orbits, while the orbits near the centre are more tangential.

Galaxy	$M_\star$	$M_\bullet$	R_e	μ_e	n	$\langle V_{\rm LOS}\rangle$	σ_e	λ_e	ϵ_e
	$[\times 10^{11} M_\odot]$	$[\times 10^{10} M_\odot]$	[kpc]	[mag/arcsec^2]		[km/s]	[km/s]		
(1)	(2)	(3)	(4)	(5)	(6)	(7)	(8)	(9)	(10)
BH-6	4.960	2×0.85	5.507	20.26	4	6.9	311	0.024	0.11
NGC 1600	5.0	1.7	~ 16	(22.53)	5.83	3.4	293	0.026	032

Table 4.4: Comparison between the physical properties of the simulated merger remnant "BH-6" and the galaxy NGC 1600. The properties described in the columns of the table are explained below, with the sources for the properties of NGC 1600 being written inside the brackets.

(1) Name of the galaxy.

(2) Total stellar mass (Thomas et al., 2016).

(3) Central black hole mass (Thomas et al., 2016).

(4) Effective radius (Thomas et al., 2016). For NGC 1600, the effective radius is changed from arc seconds to kpc by assuming that it is located at the distance of $D = 64$ Mpc (Thomas et al., 2016).

(5) Surface brightness at the effective radius.

(6) Sérsic index from the best fitting core-Sérsic profile fit (Thomas et al., 2016).

(7) Mean line-of-sight velocity inside the effective radius (Bender et al., 1994).

(8) Velocity dispersion inside the effective radius (Veale et al., 2017). For "BH-6", the given velocity dispersion is calculated from a Voronoi binned image as the mean of the velocity dispersion values of the bins located inside the effective radius.

(9) Spin parameter at the effective radius (Veale et al., 2018).

(10) For "BH-6": ellipticity of the galaxy at the effective radius; and for GC 1600: luminosity weighted ellipticity (Goullaud et al., 2018).

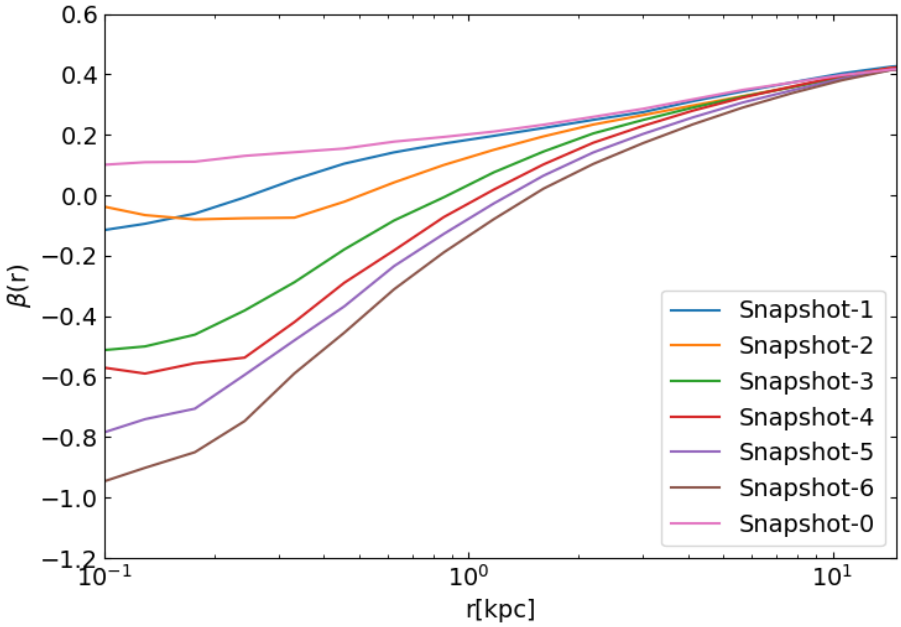

Figure 4.6: Velocity anisotropy (beta) profiles of the simulated merger remnants with central black holes.

4.5 Line-of-Sight Kinematics

4.6 Comparison to Observations

4.7 Implications

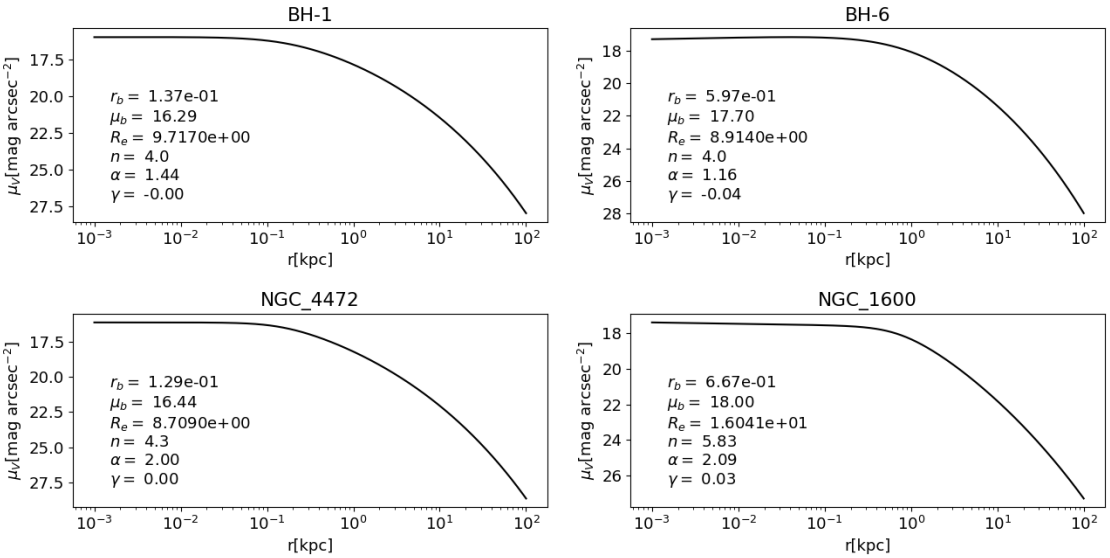

Figure 4.7: Core-Sérsic profile fits of surface brightness profiles calculated from either merger simulation results (top figures) or observed galaxies (bottom figures). The respective fit parameters are written on the figures in units that correspond to the axes. The progenitors of the top-left simulation contained $8.5 \times 10^8 M_\odot$ mass central SMBHs, and $8.5 \times 10^9 M_\odot$ mass central SMBHs in the top-right simulation. The parameters for NGC1600's profile (bottom right), are changed from the units used by Thomas et al. (2016) to the above by assuming $V - R = 0.5$ (the same assumption being done by Lauer et al. (2007b)), and by using the distance $D = 64$Mpc (Thomas et al., 2016) in order to define the relation between arc seconds and parsecs. As one can see, the profiles gained from simulations and observations are quite similar to each other.

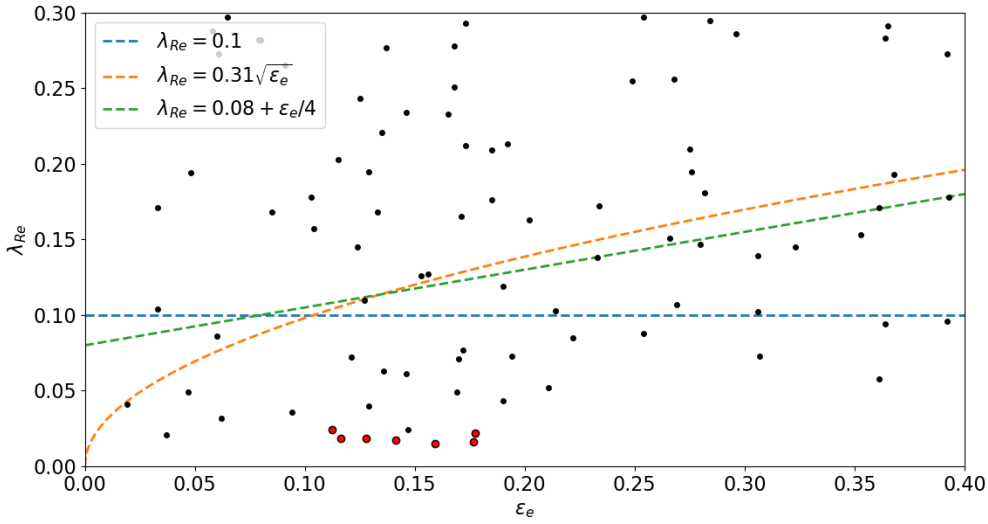

Figure 4.8: The values of the λ_{Re}-parameter of galaxies, plotted against their ellipticity at the effective radius. The red dots correspond to the simulated merger remnants, where as the black dots correspond to galaxies observed in the ATLAS^{3D}-survey (Emsellem et al., 2011). The dashed lines display different slow rotator thresholds as a function of ellipticity.

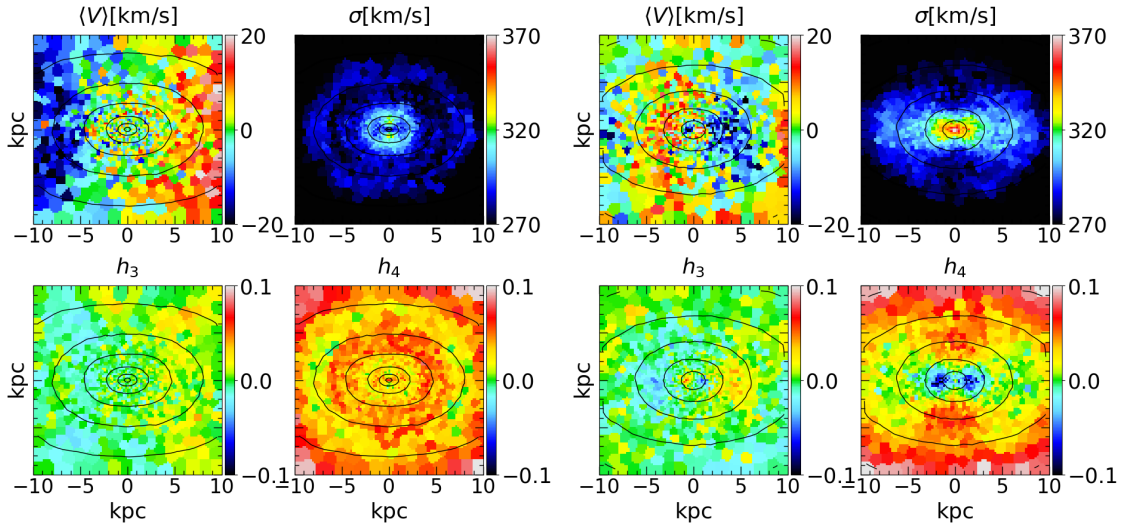

(a) BH-0 **(b)** BH-6

Figure 4.9: IFU-maps of average LOS-velocities, velocity dispersion, h_3 parameters and h_4 parameters from two simulated merger remnants. The four maps on the left are from a merger simulation where the progenitor galaxies had no central SMBHs, where as the four on the right are from a simulation with progenitor galaxies containing $M_\bullet = 8.5 \times 10^9 M_\odot$ central black holes.

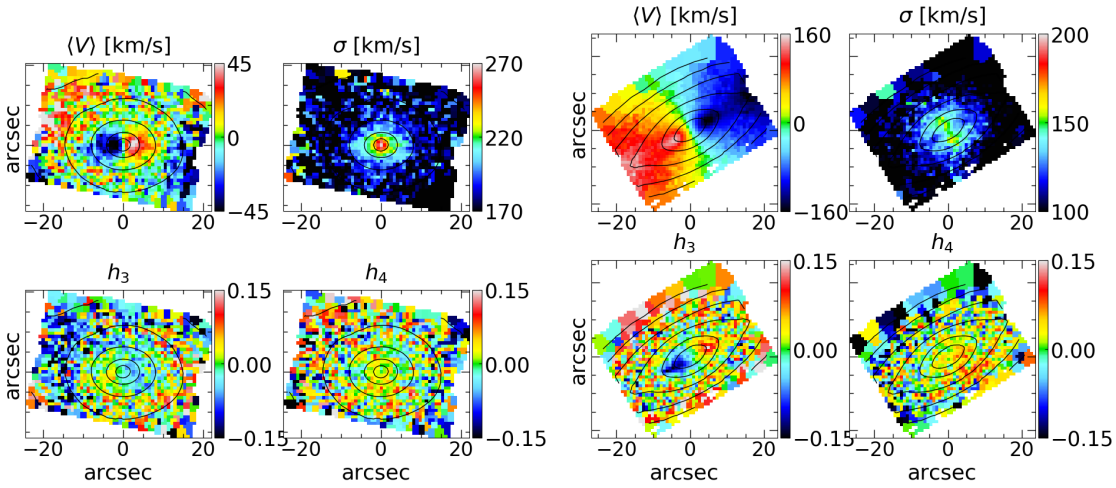

(a) NGC 3414 **(b)** NGC 4111

Figure 4.10: IFU-maps of average LOS-velocities, velocity dispersion, h_3 parameters and h_4 parameters from ATLAS3D observations of two galaxies (NGC 3414 (Emsellem et al., 2004) and NGC 4111 (Cappellari et al., 2011)).

5. Conclusions

A. Figures

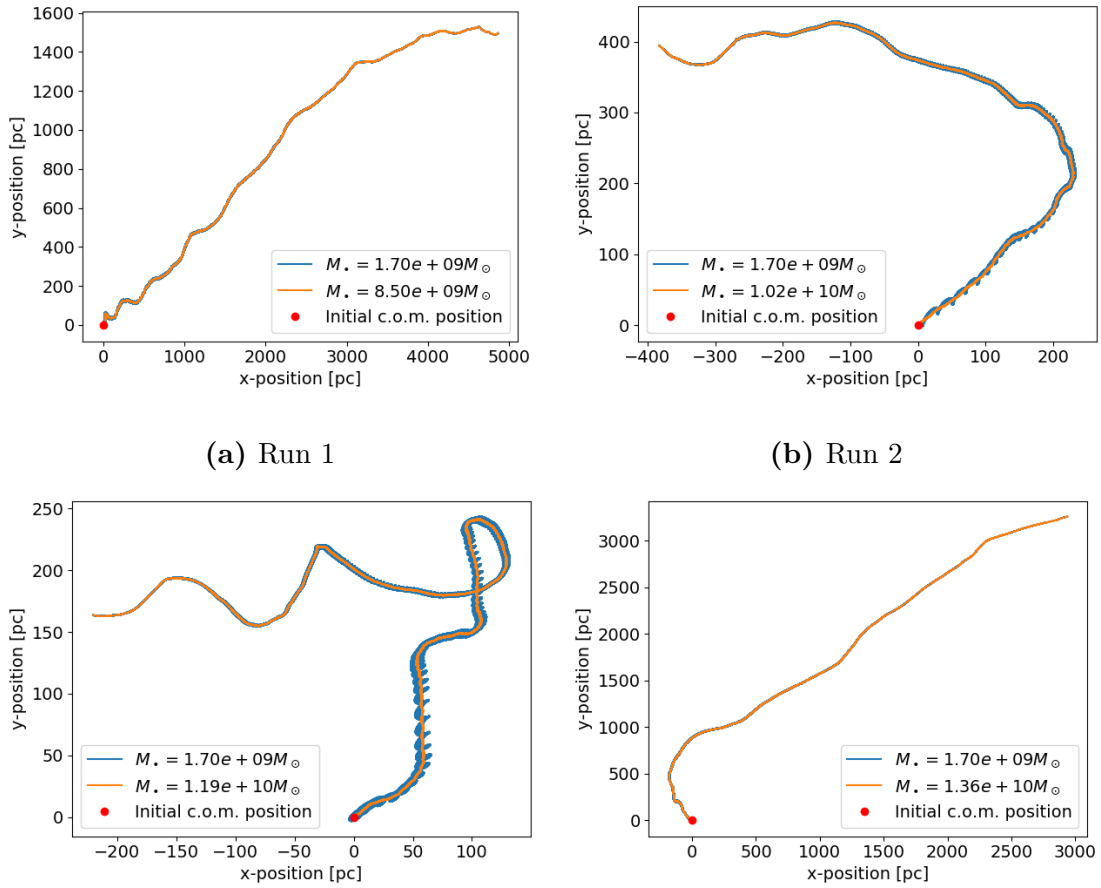

(a) Run 1 **(b)** Run 2

(c) Run 3 **(d)** Run 4

Figure A.1: The trajectories of the black holes from simulation runs by Mannerkoski et al. (2019). The coordinates are centred on the initial location of the centre-of-mass of the black hole system. The orange and blue lines show the paths taken by the smaller and larger black holes respectively during the simulation.

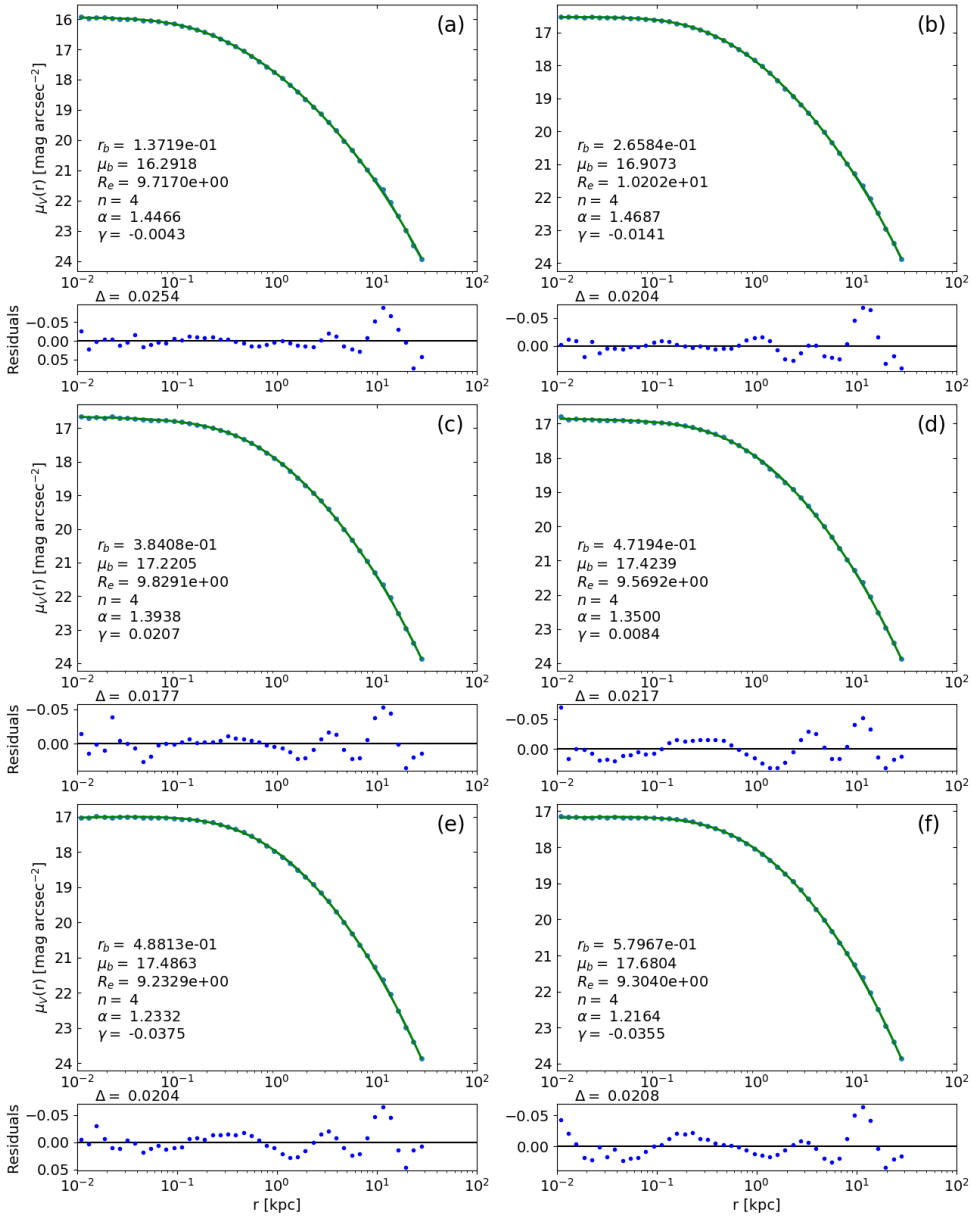

Figure A.2: Core-Sérsic profile fits of the surface brightness data calculated from all of the individual simulated merger remnants with progenitors containing central supermassive black holes. The letters (a)-(f) denote the different snapshots ((a): BH-1, (b): BH-2, (c): BH-3, (d): BH-4, (e): BH-5, (f): BH-6).

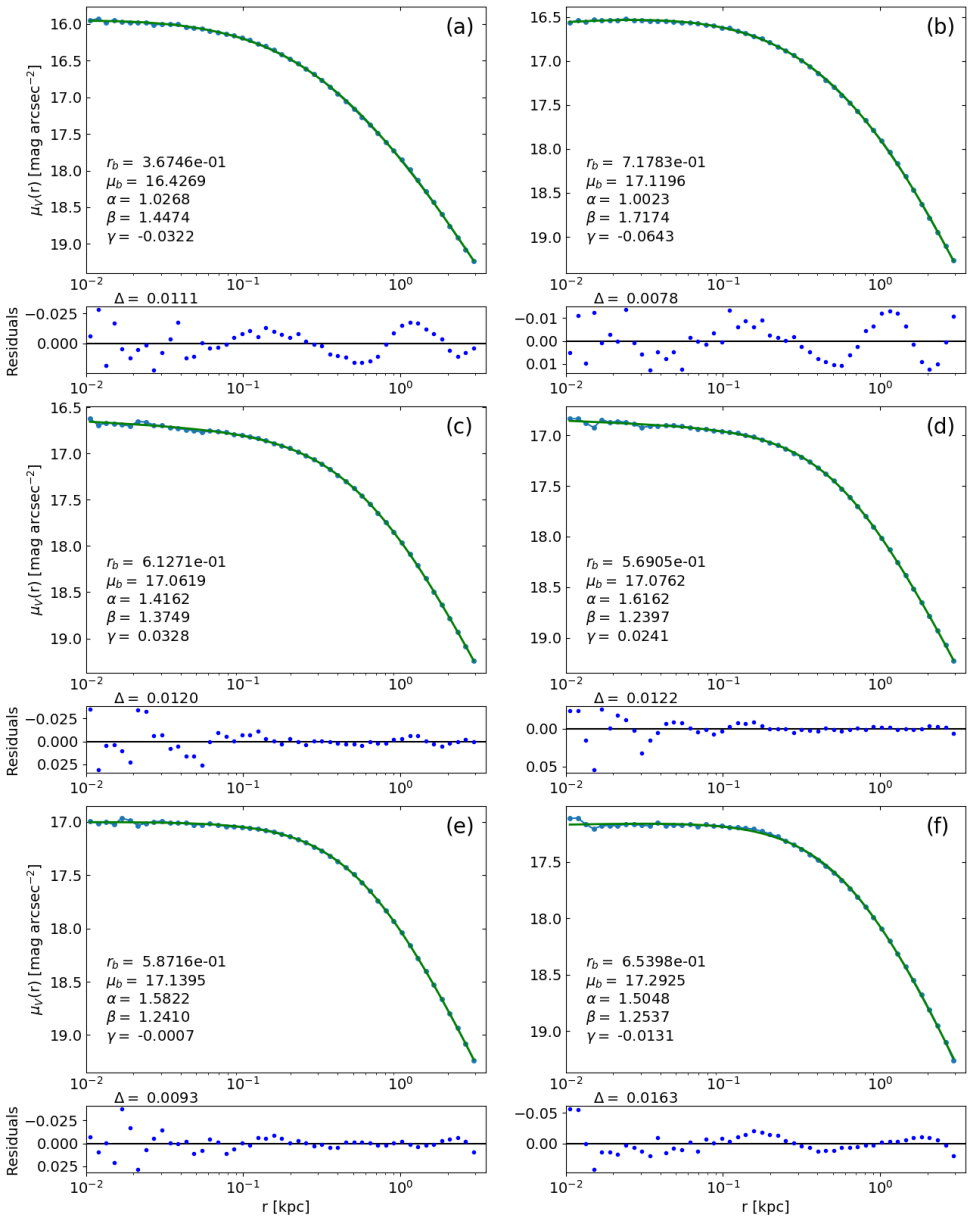

Figure A.3: Nuker profile fits of the surface brightness data calculated from all of the individual simulated merger remnants with progenitors containing central supermassive black holes. The letters (a)-(f) denote the different merger remnants ((a): BH-1, (b): BH-2, (c): BH-3, (d): BH-4, (e): BH-5, (f): BH-6).

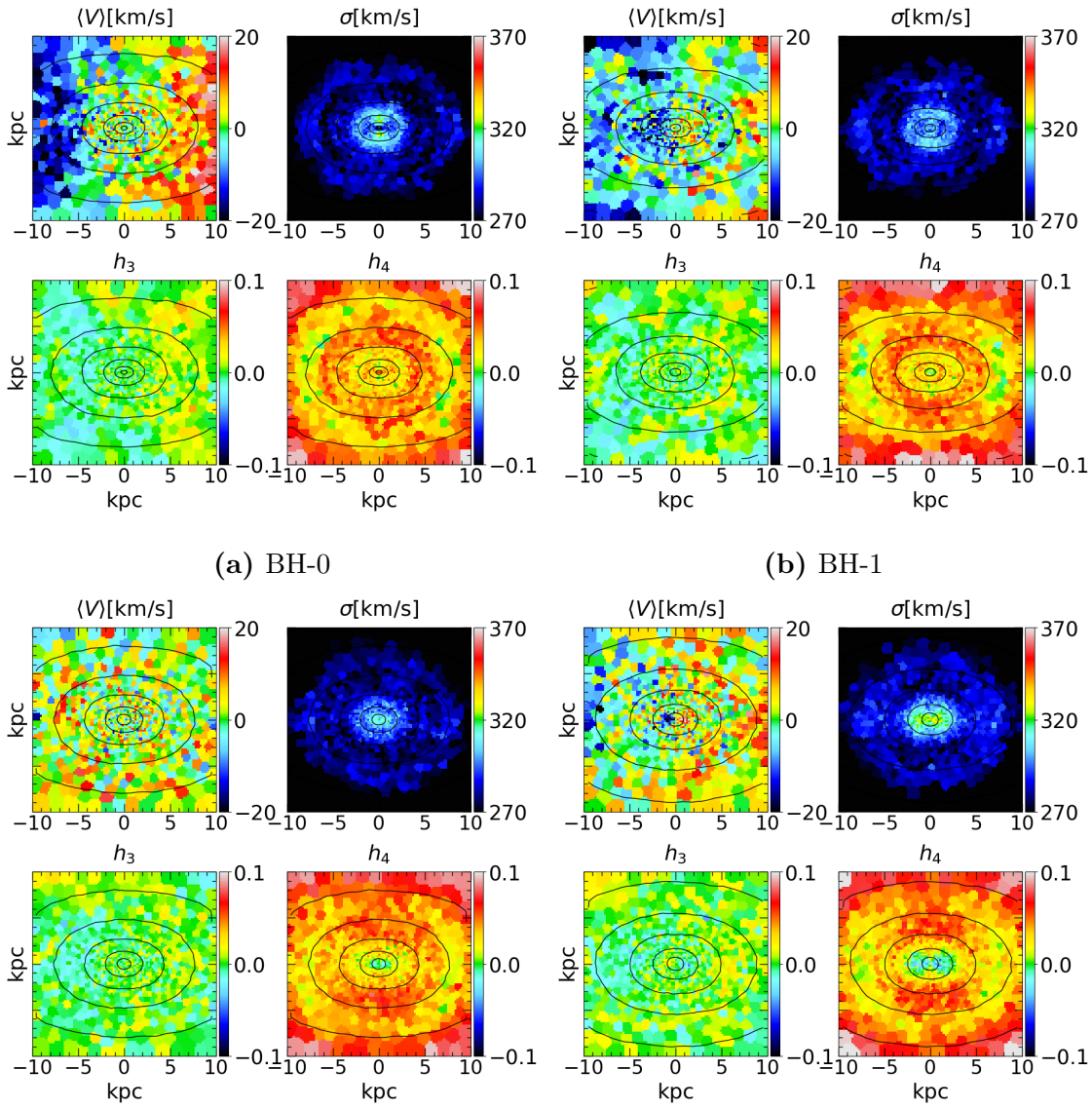

(a) BH-0 **(b)** BH-1

(c) BH-2 **(d)** BH-3

Figure A.4: IFU-maps of average LOS-velocities, velocity dispersion, h_3 parameters and h_4 parameters from four simulated merger remnants: BH-0, BH-1, BH-2 and BH-3.

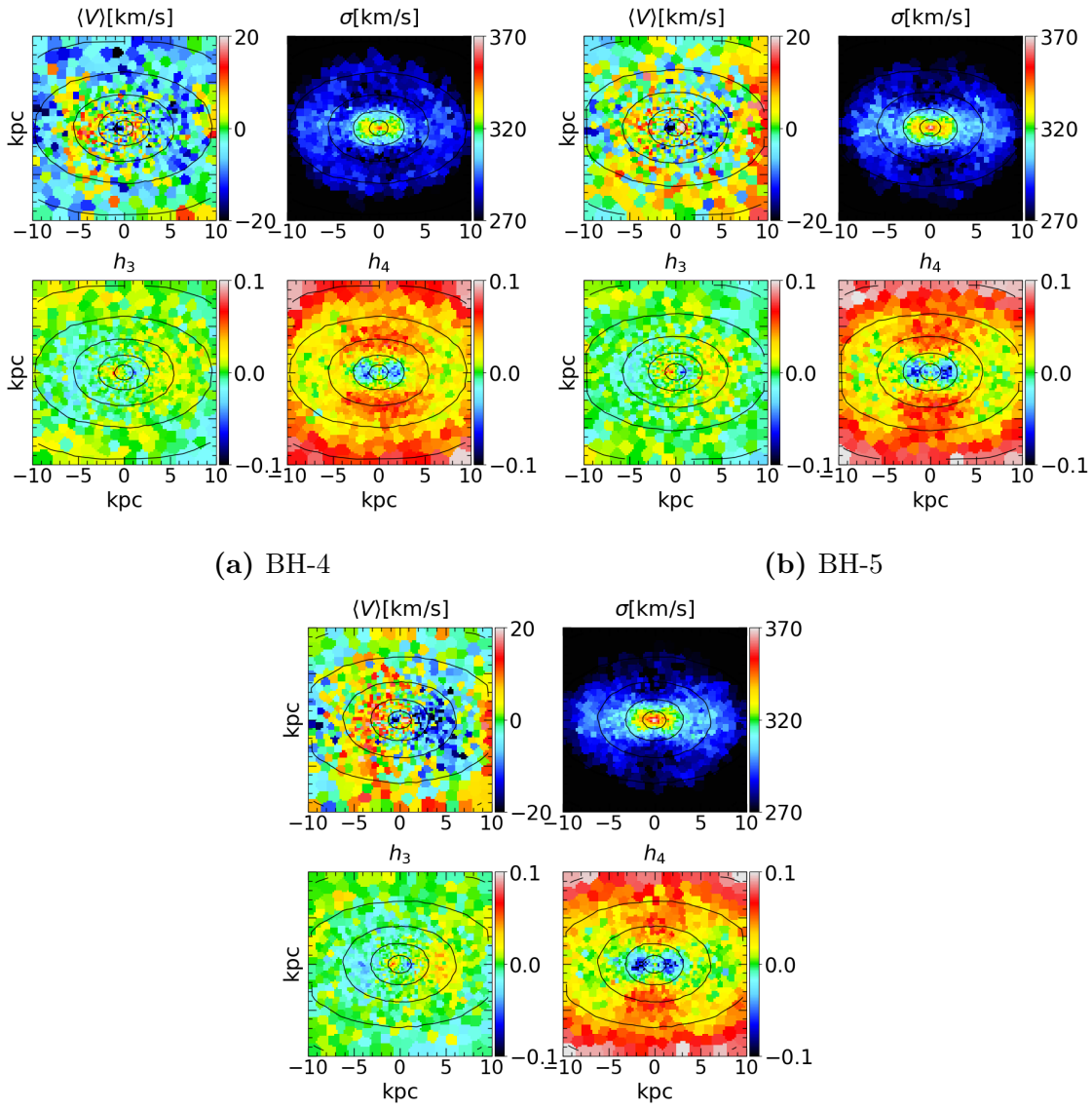

(a) BH-4

(b) BH-5

(c) BH-6

Figure A.5: IFU-maps of average LOS-velocities, velocity dispersion, h_3 parameters and h_4 parameters from three simulated merger remnants: BH-4, BH-5 and BH-6.

Bibliography

R. Bender, R. P. Saglia, and O. E. Gerhard. Line-of-sight velocity distributions of elliptical galaxies. *Monthly Notices of the Royal Astronomical Society*, 269: 785–813, Aug 1994. doi: 10.1093/mnras/269.3.785.

James Binney and Scott Tremaine. *Galactic Dynamics: Second Edition*. 2008.

M. Cappellari, E. Emsellem, D. Krajnović, R. M. McDermid, N. Scott, G. A. Verdoes Kleijn, L. M. Young, K. Alatalo, R. Bacon, L. Blitz, M. Bois, F. Bournaud, M. Bureau, R. L. Davies, T. A. Davis, P. T. de Zeeuw, P.-A. Duc, S. Khochfar, H. Kuntschner, P.-Y. Lablanche, R. Morganti, T. Naab, T. Oosterloo, M. Sarzi, P. Serra, and A.-M. Weijmans. The ATLAS^{3D} project - I. A volume-limited sample of 260 nearby early-type galaxies: science goals and selection criteria. *Monthly Notices of the Royal Astronomical Society*, 413:813–836, May 2011. doi: 10.1111/j.1365-2966.2010.18174.x.

C. Marcella Carollo, Marijn Franx, Garth D. Illingworth, and Duncan A. Forbes. Ellipticals with Kinematically Distinct Cores: V - I Color Images with WPFC2. *The Astrophysical Journal*, 481(2):710–734, May 1997. doi: 10.1086/304060.

W. Dehnen. A Family of Potential-Density Pairs for Spherical Galaxies and Bulges. *Monthly Notices of the Royal Astronomical Society*, 265:250, Nov 1993. doi: 10.1093/mnras/265.1.250.

Bililign T. Dullo and Alister W. Graham. Sizing up Partially Depleted Galaxy Cores.

The Astrophysical Journal, 755(2):163, August 2012. doi: 10.1088/0004-637X/755/2/163.

E. Emsellem, M. Cappellari, R. F. Peletier, R. M. McDermid, R. Bacon, M. Bureau, Y. Copin, R. L. Davies, D. Krajnović, H. Kuntschner, B. W. Miller, and P. T. de Zeeuw. The SAURON project - III. Integral-field absorption-line kinematics of 48 elliptical and lenticular galaxies. *Monthly Notices of the Royal Astronomical Society*, 352:721–743, August 2004. doi: 10.1111/j.1365-2966.2004.07948.x.

E. Emsellem, M. Cappellari, D. Krajnović, K. Alatalo, L. Blitz, M. Bois, F. Bournaud, M. Bureau, R. L. Davies, T. A. Davis, P. T. de Zeeuw, S. Khochfar, H. Kuntschner, P.-Y. Lablanche, R. M. McDermid, R. Morganti, T. Naab, T. Oosterloo, M. Sarzi, N. Scott, P. Serra, G. van de Ven, A.-M. Weijmans, and L. M. Young. The ATLAS^{3D} project - III. A census of the stellar angular momentum within the effective radius of early-type galaxies: unveiling the distribution of fast and slow rotators. *Monthly Notices of the Royal Astronomical Society*, 414:888–912, June 2011. doi: 10.1111/j.1365-2966.2011.18496.x.

Charles F. Goullaud, Joseph B. Jensen, John P. Blakeslee, Chung-Pei Ma, Jenny E. Greene, and Jens Thomas. The MASSIVE Survey. IX. Photometric Analysis of 35 High-mass Early-type Galaxies with HST WFC3/IR. *The Astrophysical Journal*, 856(1):11, March 2018. doi: 10.3847/1538-4357/aab1f3.

Alister W. Graham, Peter Erwin, I. Trujillo, and A. Asensio Ramos. A New Empirical Model for the Structural Analysis of Early-Type Galaxies, and A Critical Review of the Nuker Model. *The Astronomical Journal*, 125(6):2951–2963, Jun 2003a. doi: 10.1086/375320.

Alister W. Graham, Peter Erwin, I. Trujillo, and A. Asensio Ramos. A New Empirical Model for the Structural Analysis of Early-Type Galaxies, and A Critical

Review of the Nuker Model. *The Astronomical Journal*, 125(6):2951–2963, Jun 2003b. doi: 10.1086/375320.

T. R. Lauer, E. A. Ajhar, Y. I. Byun, A. Dressler, S. M. Faber, C. Grillmair, J. Kormendy, D. Richstone, and S. Tremaine. The Centers of Early-Type Galaxies with HST.I.An Observational Survey. *The Astronomical Journal*, 110:2622, Dec 1995. doi: 10.1086/117719.

Tod R. Lauer, S. M. Faber, Douglas Richstone, Karl Gebhardt, Scott Tremaine, Marc Postman, Alan Dressler, M. C. Aller, Alexei V. Filippenko, and Richard Green. The Masses of Nuclear Black Holes in Luminous Elliptical Galaxies and Implications for the Space Density of the Most Massive Black Holes. *The Astrophysical Journal*, 662(2):808–834, Jun 2007a. doi: 10.1086/518223.

Tod R. Lauer, Karl Gebhardt, S. M. Faber, Douglas Richstone, Scott Tremaine, John Kormendy, M. C. Aller, Ralf Bender, Alan Dressler, and Alexei V. Filippenko. The Centers of Early-Type Galaxies with Hubble Space Telescope. VI. Bimodal Central Surface Brightness Profiles. *The Astrophysical Journal*, 664(1):226–256, July 2007b. doi: 10.1086/519229.

Matias Mannerkoski, Peter H. Johansson, Pauli Pihajoki, Antti Rantala, and Naab Thorsten. Inspiral of Supermassive Black Holes In Galactic Scale Simulations. *Monthly Notices of the Royal Astronomical Society*, 856(1):11, ? 2019. doi: 10.3847/1538-4357/aab1f3.

Miloš Milosavljević and David Merritt. Formation of Galactic Nuclei. *The Astrophysical Journal*, 563(1):34–62, Dec 2001. doi: 10.1086/323830.

Gerald D. Quinlan and Lars Hernquist. The dynamical evolution of massive black hole binaries — II. Self-consistent N-body integrations. *New Astronomy*, 2(6):533–554, Dec 1997. doi: 10.1016/S1384-1076(97)00039-0.

Antti Rantala, Peter H. Johansson, Thorsten Naab, Jens Thomas, and Matteo Frigo. The Formation of Extremely Diffuse Galaxy Cores by Merging Supermassive Black Holes. *The Astrophysical Journal*, 864(2):113, September 2018. doi: 10.3847/1538-4357/aada47.

J. Thomas, R. P. Saglia, R. Bender, P. Erwin, and M. Fabricius. The Dynamical Fingerprint of Core Scouring in Massive Elliptical Galaxies. *The Astrophysical Journal*, 782(1):39, Feb 2014. doi: 10.1088/0004-637X/782/1/39.

Jens Thomas, Chung-Pei Ma, Nicholas J. McConnell, Jenny E. Greene, John P. Blakeslee, and Ryan Janish. A 17-billion-solar-mass black hole in a group galaxy with a diffuse core. *Nature*, 532(7599):340–342, April 2016. doi: 10.1038/nature17197.

Melanie Veale, Chung-Pei Ma, Jens Thomas, Jenny E. Greene, Nicholas J. McConnell, Jonelle Walsh, Jennifer Ito, John P. Blakeslee, and Ryan Janish. The MASSIVE Survey - V. Spatially resolved stellar angular momentum, velocity dispersion, and higher moments of the 41 most massive local early-type galaxies. *Monthly Notices of the Royal Astronomical Society*, 464(1):356–384, January 2017. doi: 10.1093/mnras/stw2330.

Melanie Veale, Chung-Pei Ma, Jenny E. Greene, Jens Thomas, John P. Blakeslee, Jonelle L. Walsh, and Jennifer Ito. The MASSIVE survey - VIII. Stellar velocity dispersion profiles and environmental dependence of early-type galaxies. *Monthly Notices of the Royal Astronomical Society*, 473(4):5446–5467, February 2018. doi: 10.1093/mnras/stx2717.